

# Measurement of the $K_S \rightarrow \gamma\gamma$ branching ratio using a pure $K_S$ beam with the KLOE detector

## The KLOE Collaboration:

*F. Ambrosino<sup>c,d</sup>, A. Antonelli<sup>a</sup>, M. Antonelli<sup>a</sup>, F. Archilli<sup>a</sup>, P. Beltrame<sup>b</sup>, G. Bencivenni<sup>a</sup>, S. Bertolucci<sup>a</sup>, C. Bini<sup>f,g</sup>, C. Bloise<sup>a</sup>, S. Bocchetta<sup>h,i</sup>, F. Bossi<sup>a</sup>, P. Branchini<sup>i</sup>, P. Campana<sup>a</sup>, G. Capon<sup>a</sup>, T. Capussela<sup>a</sup>, F. Ceradini<sup>h,i</sup>, F. Cesario<sup>h,i</sup>, P. Ciambrone<sup>a</sup>, F. Crucianelli<sup>f</sup>, S. Conetti<sup>l</sup>, E. De Lucia<sup>a</sup>, A. De Santis<sup>f,g</sup>, P. De Simone<sup>a</sup>, G. De Zorzi<sup>f,g</sup>, A. Denig<sup>b</sup>, A. Di Domenico<sup>f,g</sup>, C. Di Donato<sup>d</sup>, B. Di Micco<sup>h,i</sup>, M. Dreucci<sup>a</sup>, G. Felici<sup>a</sup>, M. L. Ferrer<sup>a</sup>, S. Fiore<sup>f,g</sup>, P. Franzini<sup>f,g</sup>, C. Gatti<sup>a</sup>, P. Gauzzi<sup>f,g</sup>, S. Giovannella<sup>a</sup>, E. Graziani<sup>i</sup>, W. Kluge<sup>b</sup>, V. Kulikov<sup>k</sup>, G. Lanfranchi<sup>a</sup>, J. Lee-Franzini<sup>a,j</sup>, D. Leone<sup>b</sup>, M. Martini<sup>a,\*</sup>, P. Massarotti<sup>c,d</sup>, S. Meola<sup>c,d</sup>, S. Miscetti<sup>a,†</sup>, M. Moulson<sup>a</sup>, S. Müller<sup>a</sup>, F. Murtas<sup>a</sup>, M. Napolitano<sup>c,d</sup>, F. Nguyen<sup>h,i</sup>, M. Palutan<sup>a</sup>, E. Pasqualucci<sup>g</sup>, A. Passeri<sup>i</sup>, V. Patera<sup>a,e</sup>, F. Perfetto<sup>c,d</sup>, P. Santangelo<sup>a</sup>, B. Sciascia<sup>a</sup>, A. Sciubba<sup>a,e</sup>, A. Sibidanov<sup>a</sup>, T. Spadaro<sup>a</sup>, M. Testa<sup>f,g</sup>, L. Tortora<sup>i</sup>, P. Valente<sup>g</sup>, G. Venanzoni<sup>a</sup>, R. Versaci<sup>a</sup>.*

<sup>a</sup>Laboratori Nazionali di Frascati dell'INFN, Frascati, Italy

<sup>b</sup>Institut für Experimentelle Kernphysik, Universität Karlsruhe, Germany

<sup>c</sup>Dipartimento di Scienze Fisiche dell'Università "Federico II", Napoli, Italy

<sup>d</sup>INFN Sezione di Napoli, Napoli, Italy

<sup>e</sup>Dipartimento di Energetica dell'Università "La Sapienza", Roma, Italy

<sup>f</sup>Dipartimento di Fisica dell'Università "La Sapienza", Roma, Italy

<sup>g</sup>INFN Sezione di Roma, Roma, Italy

<sup>h</sup>Dipartimento di Fisica dell'Università "Roma Tre", Roma, Italy

<sup>i</sup>INFN Sezione di Roma Tre, Roma, Italy

<sup>j</sup>Physics Department, State University of New York at Stony Brook, USA

<sup>k</sup>Institute for Theoretical and Experimental Physics, Moscow, Russia.

<sup>l</sup>Physics Department, University of Virginia, McCormick rd, PO Box 400714, Charlottesville, 22904, Virginia, USA.

ABSTRACT: We have searched for the decay  $K_S \rightarrow \gamma\gamma$  in a sample of  $\sim 2 \times 10^9$   $\phi \rightarrow K_S K_L$  decays collected at DAΦNE with an integrated luminosity of  $1.9 \text{ fb}^{-1}$ .  $K_S$  are tagged by the  $K_L$  interaction in the calorimeter. Two prompt photons must also be detected. Kinematic constraints reduce the initial  $6 \times 10^5$  events to 2740 candidates, from which a signal of  $711 \pm 35$  events is extracted. By normalizing to the  $K_S \rightarrow 2\pi^0$  decays counted in the same sample, we measure  $\text{BR}(K_S \rightarrow \gamma\gamma) = (2.26 \pm 0.12_{\text{stat}} \pm 0.06_{\text{syst}}) \times 10^{-6}$ , in agreement with  $\mathcal{O}(p^4)$  Chiral Perturbation Theory predictions.

KEYWORDS:  $e^+e^-$  Experiments.

---

## Contents

<b>1. Introduction</b>	<b>1</b>
<b>2. The KLOE detector</b>	<b>2</b>
<b>3. Search of <math>K_S \rightarrow \gamma\gamma</math> with a pure <math>K_S</math> beam</b>	<b>2</b>
3.1 $K_S$ tagging and event preselection	2
3.2 Kinematic fitting and event counting	4
<b>4. Branching ratio evaluation and systematics</b>	<b>7</b>
<b>5. Conclusion</b>	<b>9</b>
<b>6. Acknowledgements</b>	<b>10</b>

---

## 1. Introduction

A precise measurement of the  $K_S \rightarrow \gamma\gamma$  partial width provides a test of Chiral Perturbation Theory ( $\chi$ PT). The  $K_S \rightarrow 2\gamma$  decay amplitude has been evaluated at leading order in  $\chi$ PT,  $\mathcal{O}(p^4)$ , providing an estimate to a few percent accuracy of branching ratio (BR):  $\text{BR}(K_S \rightarrow 2\gamma) = 2.1 \times 10^{-6}$  [1]. Measurements of such BR have changed considerably with time [2, 3] while improving in precision. The latest determination comes from NA48 [4],  $\text{BR} = (2.71 \pm 0.07) \times 10^{-6}$ . This result differs by about 30% from the  $\mathcal{O}(p^4)$   $\chi$ PT estimate, possibly due to higher order corrections.

We report in the following on a measurement based on a integrated luminosity  $\int \mathcal{L} dt \sim 1.9 \text{ fb}^{-1}$  collected with the KLOE detector [5] at DAΦNE [6], the Frascati  $\phi$ -factory. DAΦNE is an  $e^+e^-$  collider operated at a center of mass energy,  $W$ , of  $\sim 1020 \text{ MeV}$ , the mass of the  $\phi$ -meson. Equal-energy positron and electron beams collide at an angle of  $(\pi - 0.025)$  radians, producing  $\phi$ -mesons nearly at rest.  $\phi$ -mesons decay 34% of the time into nearly collinear  $K^0\overline{K}^0$  pairs. Since  $J^{PC}(\phi) = 1^{--}$ , the  $K^0\overline{K}^0$  pair is in an antisymmetric state and the two kaons are always a pure  $K_S K_L$  pair. Detection of a  $K_L$ -meson therefore guarantees the presence of a  $K_S$ -meson of known momentum and direction. This procedure, called tagging, allows us to obtain a pure  $K_S$  beam. The data analyzed consists of some 2 billions  $K_S K_L$  pairs.

---

\*Corresponding author. Email address: matteo.martini@lnf.infn.it

†Corresponding author. Email address: stefano.miscetti@lnf.infn.it

## 2. The KLOE detector

The KLOE detector consists of a large cylindrical drift chamber, DC [7], of 4 m diameter and 3.3 m length operated with a low  $Z$  and density gas (helium-isoC<sub>4</sub>H<sub>10</sub>), surrounded by a lead-scintillating fiber calorimeter, EMC [8]. The chamber provides tracking, measuring momenta with a resolution of  $\delta p_{\perp}/p_{\perp}$  of 0.4% at large angle and reconstruction of two track intersections, vertices, to an accuracy of  $\sim 3$  mm. A superconducting coil around the EMC provides a 0.52 T magnetic field. The low-beta insertion quadrupoles are in the middle of KLOE. They are therefore surrounded by two compact tile calorimeters, QCAL [9], used as veto for otherwise undetected photons absorbed by the quadrupoles.

The EMC is divided into a barrel and two endcaps covering 98% of the solid angle. Modules are read out at both ends by photomultipliers, PM, with a readout granularity of  $\sim 4.4 \times 4.4$  cm<sup>2</sup> for a total of 2440 cells. The calorimeter thickness is  $\sim 15$  radiation lengths,  $X_0$ . Both amplitude and time information are obtained from the PMs. The signal amplitude measures the energy deposited in a cell and its time provides both the arrival time of particles and the position along the modules of the energy deposits, the latter by time difference. Cells close in time and space are grouped into a “calorimeter cluster”. The cluster energy  $E$  is the sum of the cell energies. The cluster time  $T$  and position  $\mathbf{R}$  are energy-weighted averages.  $\mathbf{R}$  indicates the cluster position with respect to the detector origin of coordinates. Energy and time resolutions are  $\sigma_E/E = 5.7\%/\sqrt{E \text{ (GeV)}}$  and  $\sigma_t = 57 \text{ ps}/\sqrt{E \text{ (GeV)}} \oplus 100 \text{ ps}$ , respectively. The photon detection efficiency is  $\sim 90\%$  at  $E = 20$  MeV and reaches 100% above 70 MeV.

The QCAL calorimeters,  $\sim 5X_0$  thick, have a polar angle coverage of  $0.94 < |\cos\theta| < 0.99$ . Each calorimeter consists of 16 azimuthal sectors of lead and scintillator tiles. The readout is by wavelength shifter fibers and photomultipliers. The fiber arrangement allows the measurement of the longitudinal coordinate by time differences.

Only calorimeter signals are used for the trigger [10]. Two isolated energy deposits,  $E > 50$  MeV in the barrel and  $E > 150$  MeV in the endcaps, are required. Identification and rejection of cosmic-ray events are also performed by the trigger hardware. A background rejection filter, Filfo [11], based on calorimeter information runs offline. Filfo rejects residual cosmic-ray, machine background and Bhabha events degraded by grazing the QCAL, before running event reconstruction.

## 3. Search of $K_S \rightarrow \gamma\gamma$ with a pure $K_S$ beam

### 3.1 $K_S$ tagging and event preselection

The mean  $K_S$  and  $K_L$  decay lengths in KLOE are  $\lambda_S \sim 0.6$  cm and  $\lambda_L \sim 340$  cm respectively. About 50% of the produced  $K_L$ -mesons reach the calorimeter before decaying.  $K_S$ -mesons are very cleanly tagged, with high efficiency  $\sim 30\%$ , by identifying a  $K_L$  interaction in the EMC, which we call  $K_L$ -crash. A  $K_L$ -crash has a very distinctive EMC signature: a late ( $\langle\beta_K\rangle \cong 0.22$ ) high-energy cluster with no nearby track. The average value of the  $e^+e^-$  collision center of mass energy,  $W$ , is obtained with an accuracy of 30 keV for each 100 nb<sup>-1</sup> of integrated luminosity, by reconstructing large angle Bhabha scattering

events. The mean interaction point, IP, position and the  $p_\phi$  momentum are also obtained. The value of  $W$ ,  $p_\phi$  and the  $K_L$ -crash cluster position provide, for each event, the trajectory of the  $K_S$  with an angular resolution of  $1^\circ$  and a momentum resolution better than 1 MeV. In the analyzed sample, corresponding to an integrated luminosity  $\int \mathcal{L} dt = 1.9 \text{ fb}^{-1}$ , we observe  $\sim 700 \times 10^6$  tagged  $K_S$ -mesons. Using the most recent value of  $\text{BR}(K_S \rightarrow \gamma\gamma)$  [4], we expect  $\sim 1900$  tagged  $K_S \rightarrow \gamma\gamma$  events. Because of tagging, we have no  $K_L \rightarrow 2\gamma$  background, the major contamination in the NA48 measurement. The main background in our analysis is due to  $K_S \rightarrow 2\pi^0$  events with two photons undetected because out of geometrical acceptance or not reconstructed in the EMC.

We estimate all backgrounds with the KLOE Monte Carlo, MC, [11]. We produced  $\phi$  decays to all channels corresponding to an integrated luminosity  $\int \mathcal{L} dt \sim 1.5 \text{ fb}^{-1}$ . In addition, for the signal we use a very large sample of MC  $K_S \rightarrow \gamma\gamma$  events, equivalent to  $\int \mathcal{L} dt \sim 100 \text{ fb}^{-1}$ . In the simulation, the photon detection efficiency and resolutions have been tuned with data using a large sample of tagged photons from  $\phi \rightarrow \pi^+\pi^-\pi^0$  events selected using only drift chamber information [11].  $K_L$  interactions in the EMC are also simulated.

Since the  $K_S$  decay length is approximately 1/10 the distance traveled by a photon in our time resolution we take all  $K_S$ -decay photons as originating at the IP. A prompt photon is defined as a neutral cluster in the EMC, satisfying the condition  $|T - R/c| < \min(5\sigma_t, 2\text{ns})$ , where  $T$  is the time of flight (TOF) and  $R = |\mathbf{R}|$  indicates the cluster position with respect to the detector origin of coordinates.  $\sigma_t$  is the total time resolution. After tagging, we define a signal-enriched sample by requiring two and no more than two prompt photons in the event. While the minimum energy of photons from  $K_S \rightarrow \gamma\gamma$  is 197 MeV, photons from  $K_S \rightarrow 2\pi^0 \rightarrow 4\gamma$  can be much softer,  $E_\gamma > 15.8 \text{ MeV}$ . Also at this momentum our resolution is of  $\mathcal{O}(40\%)$ . To maximize  $K_S \rightarrow 2\pi^0$  rejection we therefore consider all clusters with  $E > 7 \text{ MeV}$ , and  $|\cos(\theta)| < 0.93$ . The distribution of photons from  $K_S \rightarrow 2\pi^0$  not detected by the EMC is peaked at  $|\cos\theta|=1$ , as shown by the MC spectrum in Fig. 1.

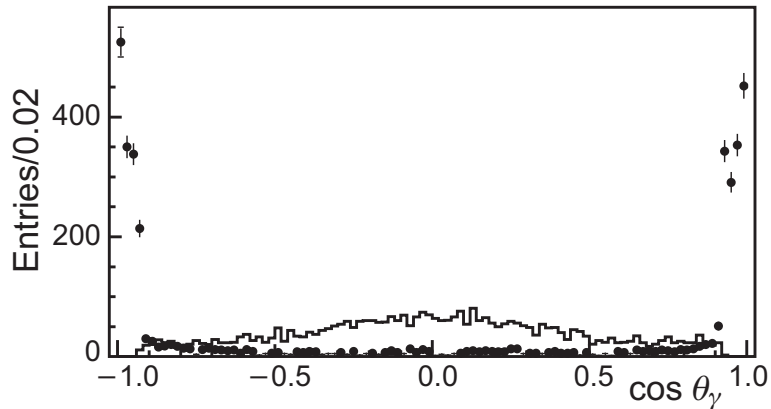


**Figure 1:** Angular distribution of photons from  $K_S \rightarrow 2\pi^0$  with two photons in the EMC. Reconstructed photons solid-line histogram, undetected photons points.

After these cuts, we are left with 550,000 events, a signal efficiency of  $\sim 83\%$  and a

signal over background ratio  $S/B \sim 1/300$ . The background is mostly from  $K_S \rightarrow 2\pi^0$  events (99.1%) and a 0.7% contamination of false  $K_L$ -crash from  $K^+K^-$  events. There is also a residual background from  $K_S$ -decays other than  $2\pi^0$ : 0.2% from  $\pi^+\pi^-$ , 0.02% from  $\pi\ell\nu$ . To improve background rejection, we veto events with photons absorbed by the QCAL. Fig. 2 shows the distribution of the difference between the reconstructed and the expected time of the QCAL signals,  $\Delta T_Q$ . The in-time peak is due to  $K_S \rightarrow 2\pi^0$  with photons reaching the QCAL.

The oscillating distribution is due to machine background events and shows the period of the beam bunches. All events having at least one hit in QCAL with energy above threshold and in a time window, TW, defined by  $|\Delta T_Q| < 5$  ns are vetoed. This veto removes  $\sim 70\%$  of the background, while retaining high efficiency for the signal. The signal loss is  $\sim 0.04\%$ .

We must however correct for the signal loss due to the accidental coincidence with machine background signals in the TW. The correction is  $C_Q = 1 - P_Q^{\text{TW}}$ , where  $P_Q^{\text{TW}}$  is the probability of a random coincidence in the TW. The latter is taken as the average of values obtained in two different out-of-time windows, one early and one late with respect to the collision time. We estimate the systematic error from the value of  $P_Q^{\text{TW}}$  obtained from reconstructed  $K_S \rightarrow \pi^+\pi^-$  decays where no photons are present. We find:  $P_Q^{\text{TW}} = (3.51 \pm 0.04_{\text{stat}} \pm 0.26_{\text{syst}})\%$ . At the end of the acceptance and QCAL veto selection, we remain with  $157 \times 10^3$  events. The S/B ratio is  $\sim 1/80$  at this stage.

### 3.2 Kinematic fitting and event counting

To improve the S/B ratio, we perform a kinematic fit imposing seven constraints: energy and momentum conservation, the kaon mass and the two photon velocities. Input variables to the fit are the IP coordinates, the  $K_S$  decay point, the  $K_S$  momentum  $|\mathbf{p}|$ , the interaction points of the two photons in the EMC and the two cluster energies. All of these 15 variables are adjusted by the fit. There is no unmeasured variable to be determined. So this is a 7-C fit with the number of degrees of freedom being  $\text{dof}=7$ . Fig. 3a, 3b and 6a, show a peak in  $\chi^2$  at  $\sim 5$  as expected for  $\text{dof}=7$ .

Fig. 3 shows the  $\chi^2$  distribution from the fit for data and MC events, after acceptance selection, before and after applying the QCAL veto. The background has high  $\chi^2$  values. Rejecting events with  $\chi^2 > 20$  we retain  $\sim 63\%$  of the signal while considerably reducing the background. The S/B ratio improves from  $1/80$  to  $1/3$ . After this cut, the background is entirely due to  $K_S \rightarrow 2\pi^0$  events with two undetected photons. Background, Fig. 4, can be further reduced using the  $\gamma\gamma$  invariant mass  $M_{\gamma\gamma}$ , and the photon opening angle in the kaon rest frame,  $\theta_{\gamma\gamma}^*$ . Since the kinematic fit imposes the kaon mass as a constraint, we

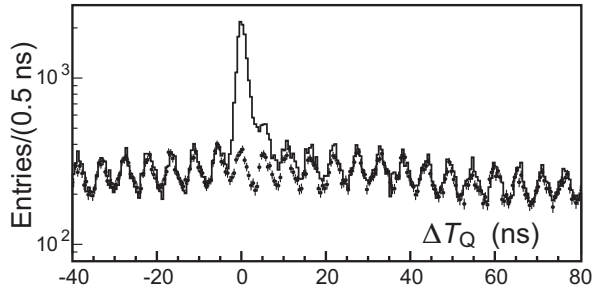


**Figure 2:** Inclusive distribution of the difference between the measured arrival time and the expected time of flight of hits in QCAL for events tagged by a  $K_L$ -crash with two prompt photons (solid line) or with a reconstructed  $K_S \rightarrow \pi^+\pi^-$  decay (points).

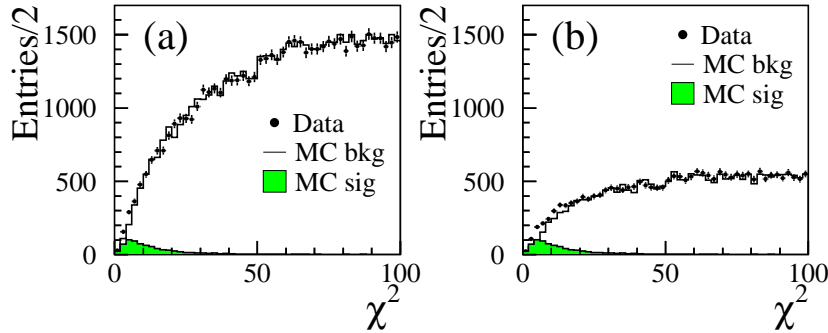


**Figure 3:**  $\chi^2$  distributions for tagged  $K_S$  events with two prompt photons: before (a) and after (b) QCAL veto.

use the measured variables values before fitting. Fig. 4 shows plots of  $M_{\gamma\gamma}$  vs  $\cos\theta_{\gamma\gamma}^*$  for data, MC background and MC signal events.

To check the MC description of the EMC as a function of the photon energy, we inspect the energy pulls of the kinematic fit for  $2\pi^0$   $K_S$  decays. We use a data sample corresponding to  $\int \mathcal{L} dt \sim 80 \text{ pb}^{-1}$  and equal MC statistics. We select tagged  $K_S$ -mesons and ask for four prompt photons. An energy scale correction of  $\sim 1.02$  is required to improve the match between MC simulation and data. After applying this correction, the MC ability to reproduce signal spectra is tested with a control sample of  $K_L \rightarrow \gamma\gamma$  events decaying near the beam pipe, with the  $K_L$ -meson tagged by a well reconstructed  $K_S \rightarrow \pi^+\pi^-$  decay. The BR for  $K_L \rightarrow 2\gamma$  is  $5.74 \times 10^{-4}$  which together with the lifetime,  $\tau_{K_L} = 5.08 \times 10^{-8}$  corresponds to an equivalent  $\text{BR}(K_L \rightarrow 2\gamma)$  of  $1.6 \times 10^{-6}$  per cm of  $K_L$  path. Thus decays within 30 cm of the IP provide a sample of  $K_L \rightarrow 2\gamma$  larger than that of  $K_S \rightarrow 2\gamma$  and with a background level from  $2\pi^0$  decays smaller by three orders of magnitude. The  $K_L$  vertex position is calculated by knowing the  $K_L$  flight direction and the time of flight of the two photons with a precision of  $\sim 1.5 \text{ cm}$ .

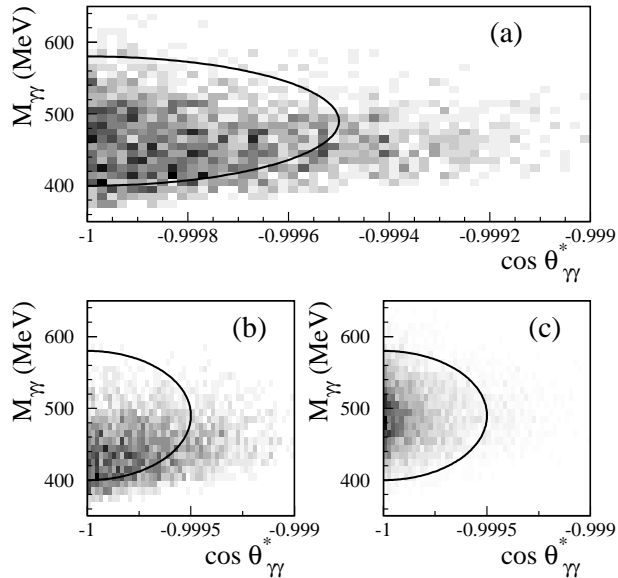


**Figure 4:** Scatter plot of  $M_{\gamma\gamma}$  vs  $\cos\theta_{\gamma\gamma}^*$ , after pre-selection, for data (a), MC background (b) and MC signal (c). The solid curve represents the signal dominated region.

Data (MC) corresponding to  $\int \mathcal{L} dt = 200$  (450)  $\text{pb}^{-1}$  are used. Events are selected as for the  $K_S \rightarrow 2\gamma$  decays, including the kinematic fit. The background is negligible after requiring  $\chi^2 < 20$ . A gaussian fit to the  $M_{\gamma\gamma}$  distributions is shown in Fig. 5. Data and

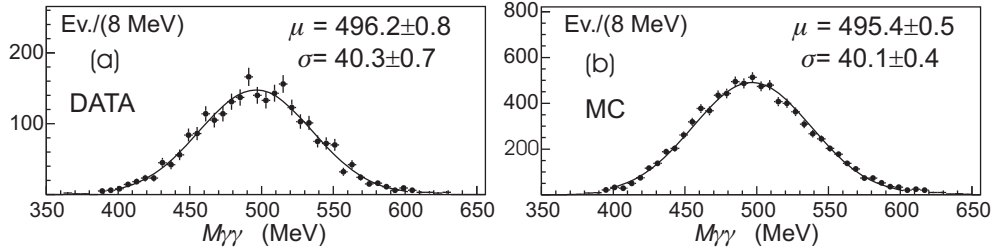


**Figure 5:**  $\gamma\gamma$  invariant mass for the  $K_L \rightarrow \gamma\gamma$  decays near the beam pipe.

MC energy scales agree to better than 0.2%,  $\sim 1/5$  of the error which is quite satisfactory. The resolution agrees to 2%. The  $\chi^2$  and  $\cos \theta_{\gamma\gamma}^*$  distributions of the  $K_L$  events, Fig. 6 a and b, confirm the simulation results for  $K_S \rightarrow 2\gamma$  decays.

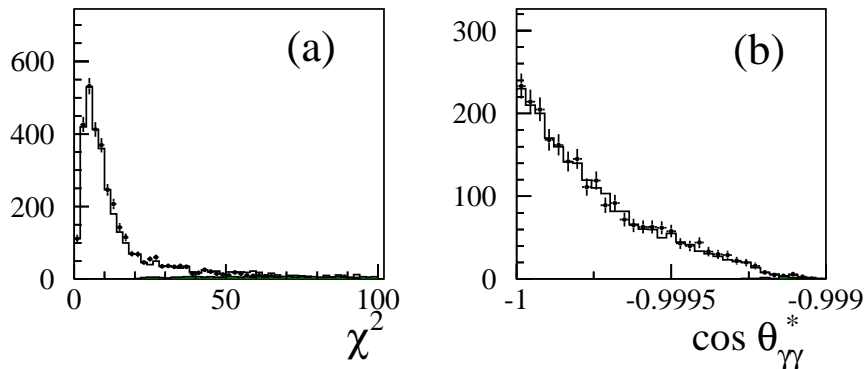


**Figure 6:** Distributions of  $\chi^2$  (a) and  $\cos \theta_{\gamma\gamma}^*$  (b) for  $K_L \rightarrow \gamma\gamma$  decays near the IP. Black points are data, grey histogram is the MC simulation. The plot of  $\chi^2$  has been done with preselection cuts on the two photons and a cut on  $\cos \theta_{\gamma\gamma}^*$  below -0.998. The  $\cos \theta_{\gamma\gamma}^*$  distribution required a  $\chi^2$  cut at 20.

To obtain the number of  $K_S \rightarrow 2\gamma$  events, we perform a 2 dimensional binned-maximum-likelihood of the the final sample distribution in the  $M_{\gamma\gamma}$  and  $\cos \theta_{\gamma\gamma}^*$  variables. The likelihood function uses the MC generated signal and background shapes taking into account data and MC statistics. The fit gives  $N(\gamma\gamma) = 711 \pm 35$ , with a  $\chi^2/\text{dof} = 854/826$ . The fit CL is 24.3%.

Projections of data and fit are shown in Fig. 7. The signal  $\cos \theta_{\gamma\gamma}^*$  distribution is peaked at  $\cos \theta = -1$  while the  $M_{\gamma\gamma}$  distribution is gaussian at the  $K_S$  mass. The background is less peaked at  $\cos \theta = -1$  and lower and broader in mass. As an independent check of the fit quality, we show in Fig. 8.a the  $\chi^2$  distribution for data and MC after minimization. A similar comparison is done also for the angular photon spectrum (Fig. 8.b),

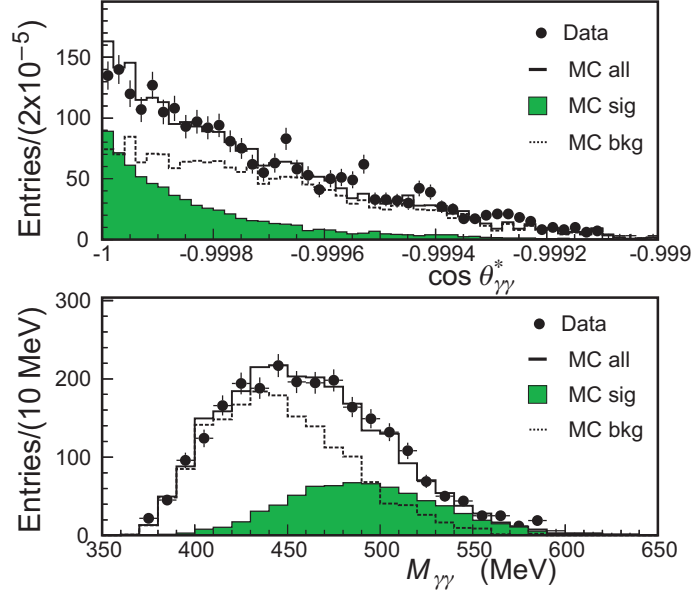


**Figure 7:** Distributions of  $\cos(\theta_{\gamma\gamma}^*)$  (a) and  $M_{\gamma\gamma}$  (b) for the final sample.

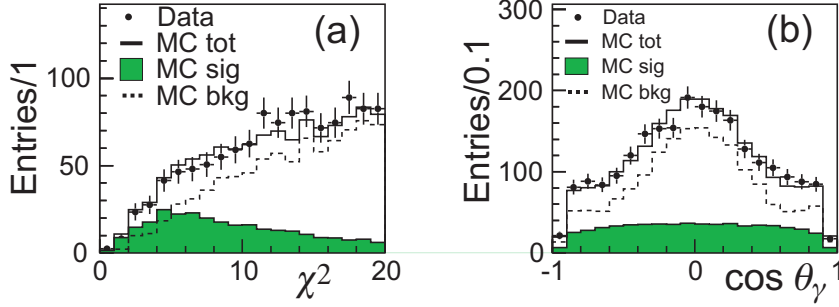


**Figure 8:** Distributions of  $\chi^2$  (a) and inclusive  $\cos\theta_\gamma$  of the two photons in the event (b) for the final sample.

which clearly indicates the presence of a flat component due to signal, as expected for the two body decay of a spin 0 particle.

#### 4. Branching ratio evaluation and systematics

The branching ratio is obtained from  $N(K_S \rightarrow \gamma\gamma)$  using for normalization the yield for  $K_S \rightarrow 2\pi^0$  in the same sample of tagged  $K_S$ -mesons by counting events with four prompt photons:

$$\text{BR}(K_S \rightarrow 2\gamma) = \frac{N(K_S \rightarrow \gamma\gamma)}{N(K_S \rightarrow 2\pi^0)} \times \frac{\epsilon_{\text{TOT}}(2\pi^0|\text{tag})}{\epsilon_{\text{TOT}}(\gamma\gamma|\text{tag})} \times \text{BR}(K_S \rightarrow 2\pi^0) \times R_\epsilon \quad (4.1)$$

The total efficiencies have been evaluated by MC after  $K_L$ -crash tag. The signal total efficiency is the product of the efficiencies for the acceptance selection, the QCAL cut and the  $\chi^2$  cut:

$$\epsilon_{\text{TOT}}(\gamma\gamma) = \epsilon_{\text{sel}}(\gamma\gamma) \times \epsilon_{\text{Q}}(\gamma\gamma) \times \epsilon_{\chi^2}(\gamma\gamma). \quad (4.2)$$

For the normalization sample, the efficiency is related only to the acceptance of four photons. The ratio,  $R_\epsilon$ , of all other efficiencies (triggering, Filfo filter and tagging) between signal and normalization sample should be identically one. From MC we find  $R_\epsilon = 1.001 \pm 0.001_{\text{stat}}$ . The difference from unity is added as contribution to the systematic error on the BR.

For the signal selection efficiency we find:

$$\epsilon_{\text{sel}}(\gamma\gamma) = (82.9 \pm 0.2_{\text{stat}} \pm 0.2_{\text{syst}})\%. \quad (4.3)$$

The large selection efficiency is due to the wide angular coverage of the calorimeter, the low energy threshold used and the almost flat angular distribution of the decay products. The systematic error assigned to this efficiency has been found by varying the data-MC correction of the cluster reconstruction efficiency. The efficiency for the QCAL cut is found from MC to be  $\epsilon_Q^{\text{MC}}(2\gamma) \sim 99.96\%$ . Applying the correction due to accidental losses described in sec. 3.1 we obtain:

$$\epsilon_Q(2\gamma) = \epsilon_Q^{\text{MC}}(2\gamma) \times C_Q = (96.45 \pm 0.04_{\text{stat}} \pm 0.26_{\text{syst}})\%. \quad (4.4)$$

The MC efficiency of the  $\chi^2$  cut is  $\epsilon_{\chi^2} = (63.3 \pm 0.7)\%$ . The systematic error related to the knowledge of the data–MC difference in the  $\chi^2$  scale has been evaluated by using the  $K_L \rightarrow \gamma\gamma$  control sample. For the chosen  $\chi^2$  cut, we evaluate the data over MC ratio,  $R_\chi$ , of the  $\chi^2$  cumulative distributions and we get  $(R_\chi - 1) = (-0.5 \pm 1.8)\%$ . We conservatively assign the error on  $R$  as the contribution of the  $\chi^2$  scale to the systematic error.

Source	+ $\Delta\text{BR}/\text{BR}$ (%)	- $\Delta\text{BR}/\text{BR}$ (%)
Trigger, Filter, Tag	0.10	0.10
Signal acceptance	0.17	0.17
QCAL veto	0.02	0.26
$\chi^2$ scale	1.80	1.80
Background shape	1.04	0.98
QCAL TW change	0.53	0.49
$\chi^2$ change	0.99	—
MC Energy scale	—	0.79
2D-Fit binning	0.96	0.98
Normalization sample	0.15	0.15
Total	2.56	2.48

**Table 1:** Breakdown of the contributions to the total systematic error for the BR( $K_S \rightarrow \gamma\gamma$ ).

The systematic uncertainties connected to the signal counting have been evaluated by repeating the analysis and the fit in different ways. The most delicate point is related to the simulation of the background shape. The MC shows a good agreement with data for background-enriched samples obtained by requiring a complementary cut on  $\chi^2$ , such as  $30 < \chi^2 < 500$ . Moreover, to test the fit stability in different regions of the  $M_{\gamma\gamma} - \cos\theta_{\gamma\gamma}^*$  plane, we have determined how much the result varies when: (1) reducing the fit-region

along the  $\cos\theta_{\gamma\gamma}^*$  axis moving the lower boundaries from 0.999 to 0.9995 or (2) fitting only in a signal dominated region shown by the ellipse in Fig. 4. The maximum variation of the BR for these tests is reported as background shape in Tab. 1.

We have also tested the stability of the branching ratio when modifying the width of the time window used for the QCAL veto from  $\pm 5$  ns to  $\pm 4$ ,  $\pm 6$  ns. Similarly, the cut in  $\chi^2$  has been changed from 20 to 10 and 24. We have then repeated the fit by applying to the MC an energy-scale correction of +0.4%, a factor of two larger than what measured with the  $K_L \rightarrow \gamma\gamma$  control sample. We have also checked that regrouping the bins of the 2-D plot by factors from 2 to 5 does not modify substantially the result. For all of these cases, the maximum variation of the BR obtained is used as systematic error and shown in Tab. 1. The sum in quadrature of all entries is used as total systematic error.

For the normalization we count  $K_S \rightarrow 2\pi^0$  tagged events with four prompt photons. An efficiency of

$$\epsilon_{\text{sel}}(2\pi^0) = (65.0 \pm 0.2_{\text{stat}} \pm 0.1_{\text{syst}})\% \quad (4.5)$$

is found by MC. As for the signal, the systematic uncertainty related to the cluster detection efficiency is evaluated by varying the data-MC correction curves. After correcting for  $\epsilon_{\text{sel}}(2\pi^0)$ , a number of  $(190.5 \pm 0.2) \times 10^6$   $K_S \rightarrow 2\pi^0$  tagged events is obtained. The systematic uncertainty related to the presence of machine background clusters, fragmentation and merging of clusters is estimated by repeating the measurement in an inclusive way and counting tagged events with 3, 4 and 5 photons. The overall systematic error for the normalization sample is reported in Tab. 1.

To evaluate  $\text{BR}(K_S \rightarrow \gamma\gamma)$  we use the latest PDG [12] value  $\text{BR}(K_S \rightarrow 2\pi^0) = (30.69 \pm 0.05)\%$ . See also [13]. We obtain:

$$\text{BR}(K_S \rightarrow \gamma\gamma) = (2.26 \pm 0.12_{\text{stat}} \pm 0.06_{\text{syst}}) \times 10^{-6}. \quad (4.6)$$

We have repeated the measurement by subdividing the data in two sets to check stability for the slightly different running conditions: 1)  $0.4 \text{ fb}^{-1}$  from 2001-2002 and 2)  $1.5 \text{ fb}^{-1}$  for 2004-2005. Also the simulation has been divided accordingly. We get  $\text{BR}(K_S \rightarrow \gamma\gamma) = (2.24 \pm 0.30_{\text{stat}}) \times 10^{-6}$  in 2001-2002 and  $\text{BR}(K_S \rightarrow \gamma\gamma) = (2.26 \pm 0.13_{\text{stat}}) \times 10^{-6}$  in 2004-2005, which are in excellent agreement.

Fig. 9 shows our result and other existing measurements of  $\text{BR}(K_S \rightarrow \gamma\gamma)$  as well as the  $\mathcal{O}(p^4)$   $\chi$ PT theoretical prediction. There is a  $3 \sigma$ 's discrepancy between the present result and the measurement of NA48.

## 5. Conclusion

From  $\sim 2$  billion  $\phi$  mesons collected with KLOE at DAΦNE, we have measured the  $\text{BR}(K_S \rightarrow \gamma\gamma)$  with a 5.3% statistical uncertainty and a  $\sim 2\%$  systematic error. We obtain a BR result which deviates by  $3 \sigma$ 's from the previous best determination. Precise  $\chi$ PT theory calculation for this decay are done at  $\mathcal{O}(p^4)$ . Higher order effects are predicted to be at most of the order of  $\sim 20\%$  of the  $\mathcal{O}(p^4)$  decay amplitude. Our measurement is consistent with negligible higher order corrections.

## 6. Acknowledgements

We thank the DAΦNE team for their efforts in maintaining low background running conditions and their collaboration during all data-taking. We want to thank our technical staff: G.F. Fortugno and F. Sborzacchi for their dedicated work to ensure an efficient operation of the KLOE Computing Center; M. Anelli for his continuous support to the gas system and the safety of the detector; A. Balla, M. Gatta, G. Corradi and G. Papalino

for the maintenance of the electronics; M. Santoni, G. Paoluzzi and R. Rosellini for the general support to the detector; C. Piscitelli for his help during major maintenance periods. This work was supported in part by EURODAPHNE, contract FMRX-CT98-0169; by the German Federal Ministry of Education and Research (BMBF) contract 06-KA-957; by the German Research Foundation (DFG), 'Emmy Noether Programme', contracts DE839/1-4; by DOE grant DE-FG-02-97ER41027; and by the EU Integrated Infrastructure Initiative HadronPhysics Project under contract number RII3-CT-2004-506078.

## References

- [1] G. D'Ambrosio, D. Espriu, *Phys. Lett.* **B 175** (1986) 237  
J.L. Goity, *Z. Physik* **C 34** (1987) 341  
F. Buccella, G. D'Ambrosio and M. Miragliuolo, *Nuovo Cim.* **A104** (1991) 777  
J. Kambor and B.R. Holstein, *Phys. Rev.* **D 49** (1994) 2346.
- [2] G. D. Barr, *et al.* (NA31 Collaboration), *Phys. Lett.* **B 351** (1995) 579.
- [3] A. Lai, *et al.* (NA48 Collaboration), *Phys. Lett.* **B 493** (2000) 29.
- [4] A. Lai, *et al.* (NA48 Collaboration), *Phys. Lett.* **B 551** (2003) 7.
- [5] KLOE collaboration, LNF-92/019(IR) (1992) and LNF-93/002(IR) (1993).
- [6] S. Guiducci, P. Lucas, S. Weber (Eds.), DAΦNE operating experience, Proceedings of the 2001 Particle Accelerator Conference, Chicago, IL, USA, 2001.
- [7] M. Adinolfi *et al.* (KLOE collaboration), *Nucl. Instrum. Meth.* **A488** (2002) 51.
- [8] M. Adinolfi *et al.* (KLOE collaboration), *Nucl. Instrum. Meth.* **A482** (2002) 364.
- [9] M. Adinolfi *et al.* (KLOE collaboration), *Nucl. Instrum. Meth.* **A483** (2002) 649
- [10] M. Adinolfi *et al.* (KLOE collaboration), *Nucl. Instrum. Meth.* **A492** (2002) 134.
- [11] M. Adinolfi *et al.* (KLOE collaboration), *Nucl. Instrum. Meth.* **A534** (2004) 403.
- [12] W.M.Yao *et al.*, W.-M. Yao. *et al.* (Particle Data Group), *J. Phys.* **G 33** (2006) 1 <sup>1</sup>.
- [13] F. Ambrosino, *et al.* (KLOE Collaboration), *Eur. Phys. J.* **C 48** (2006) 767.

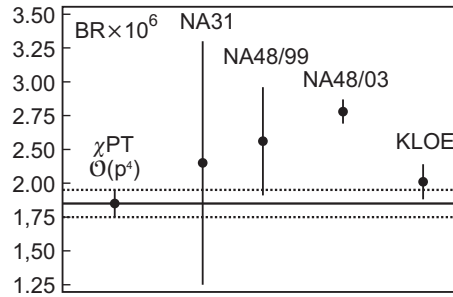


**Figure 9:** Comparison of  $\text{BR}(K_S \rightarrow \gamma\gamma)$  measurements and  $\chi_{\text{PT}}$  predictions.

<sup>1</sup>The value of  $\text{BR}(K_S \rightarrow 2\pi^0)$  is completely dominated by the KLOE results, [13]